ACS Biomaterials SCIENCE & ENGINEERING

pubs.acs.org/journal/abseba

Article

Macroporous 3D Scaffold with Self-Fitting Capability for Effectively Repairing Massive Rotator Cuff Tear

Liren Wang, Yuhao Kang, Sihao Chen, Xiumei Mo, Jia Jiang, Xiaoyu Yan, Tonghe Zhu,* and Jinzhong Zhao*

Cite This: *ACS Biomater. Sci. Eng.* 2021, 7, 904−915

Read Online

ACCESS | Metrics & More | Article Recommendations | Supporting Information

ABSTRACT: The postoperative retear rate of direct repair of massive rotator cuff tear has risen up to 40% because of the dissatisfied tendon-to-bone healing and poor regenerative potential of remnant rotator cuff tissue. A biological scaffold that connects the remnant rotator cuff tissue and bone might be a promising substitute. In the present study, we have developed a macroporous three-dimensional scaffold poly(ester-urethane)urea (PEUU), with self-fitting capability employing thermally induced phase separation (TIPS) technique. The scaffold provides oriented connected macropores for cells migration, and promoted tendon-to-bone healing on the basis of surgical repair. The scaffolds were characterized by scanning electron microscopy, stress−strain test and cell biocompatibility study. In vitro studies exhibited that PEUU scaffold with suitable elastic mechanical properties can better support proliferation and migration of rabbit bone mesenchymal stem cells (RBMSCs). After three months postreconstruction of massive rotator cuff tear in a rabbit model using PEUU scaffold, there was complete regeneration of rotator cuff with physical tendon-to-bone interface and continuous tendon tissue, as observed from histological analysis. Further, biomechanical testing demonstrated that rotator cuff induced by PEUU scaffold had no significant difference as compared to normal rotator cuff. This macroporous, mechanically matched scaffold is potentially suitable for the application in massive rotator cuff repair. In conclusion, this study demonstrates the high efficiency of the macroporous 3D scaffold with self-fitting capability in facilitating rotator cuff regeneration.

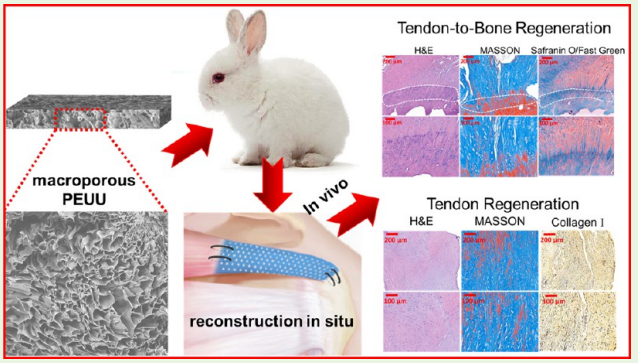

KEYWORDS: *poly(urethane urea)ester, macroporous scaffold, biomechanically matched, bridging model, massive rotator cuff tear, tendon−bone interface*

Downloaded via DONGHUA UNIV LIB on June 1, 2021 at 07:18:56 (UTC).
See https://pubs.acs.org/sharingguidelines for options on how to legitimately share published articles.

1. INTRODUCTION

Massive rotator cuff tears (MRCT) are very common devastating health issues in elder people with age over 60 and the treatment of MRCT is highly expensive. While, surgery remains the only option for the treatment of MRCT, its failure chances in terms of retear rate have risen up to 40%.[1−3] The reasons for postoperative retear could be attributed to the dissatisfied tendon-to-bone healing as well as poor regenerative potential of remnant rotator cuff tissue.[4,5]

The high percentage of surgery failure has facilitated the urgency to find a new alternative solution that can overcome the limitations associated with conventional treatment strategy of MRCT. In this context, biological scaffold, which builds bridge between remnant rotator cuff tissue and bone, might be a promising substitute for MRCT regeneration.[6−8] Biodegradable scaffolds are considered as excellent materials for rotator cuff regeneration with high surface/volume ratio, tunability, and flexibility to prepare a tissue engineering scaffold possessing microstructure similar to native tissue. Polycaprolactone (PCL) is a biodegradable and biocompatible material with proper mechanical property and previous reports demonstrated the development of tendon structure mimicking PCL-based composite as rotator cuff augmentation patches.[9−12] Orr SB found that compared with multilayered nonaligned scaffolds, not only was the mechanical property improved but the expression of tenomodulin was enhanced in multilayered aligned scaffolds as well.[11] To improve the hydrophilicity of PCL scaffold, we used PCL−chitosan scaffolds to for rotator cuff regeneration in our previous study.[12] Enhanced bone, tendon-to-bone, and tendon formation were observed 3 months after implantation. However, infiltration and adhesion of tendon cells and bone marrow stem cells (BMSCs) was difficult with the PCL scaffolds.[13,14]

Special Issue: Innovations in Orthopedic Biomaterials and Regenerative Medicine in China

Received: February 6, 2020
Accepted: April 13, 2020
Published: April 13, 2020

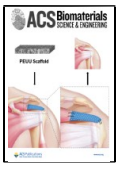

ACS Publications © 2020 American Chemical Society

Application of poly(ester-urethane)urea (PEUU) scaffold was emphasized. Nair et al. found that both the material and the degradation products of PEUU scaffold were noncytotoxic.[15] Consisting of extracellular matrix gel and PEUU nanofiber, a biohybrid composite was generated for a full-thickness abdominal wall defect, and 4 weeks after implantation, no infection was observed at the implant site.[16] However, few studies have reported PEUU application in rotator cuff tissue engineering.

Recent studies also concentrated on pore size and three-dimensional (3D) structure of scaffolds to facilitate the cellular penetration and tissue in growth.[17−19] However, biocompatibility of the scaffold for tissue regeneration would be significantly differed when organic solvents or particulate leaching was included. Porous scaffolds can be fabricated by the thermally induced phase separation (TIPS) technique without remnant solvents, preserving the biocompatibility of the scaffold. TIPS parameters, including polymer type and concentration, solvent or nonsolvent ratio, and the cooling rate, can be adjusted for distinctive scaffold with unique porosity tailored for various utilization. A porous scaffold fabricated by TIPS has been recently used in myocardial, dermal, and bone tissue regeneration.[20−22] Nevertheless, the enhanced level of porosity in the microstructure of scaffolds is generally accompanied by the reduction of mechanical strength, resulting from large void space.[23] Via infinite element simulation, Zhang et al. found that the Young's moduli of scaffolds decreased linearly with increasing scaffold porosity.[24] For cartilage regeneration, soft and porous scaffolds are much preferred compared with stiff scaffold.[25] Because cartilage regeneration is highly critical for tendon-to-bone regeneration, a soft and porous scaffold that prevents scaffold breakage during degeneration and regeneration might be ideal for rotator cuff scaffold.

In the present study, we have employed the TIPS method to fabricate a suitable rotator cuff regenerating novel scaffold within an oriented, interconnected, and porous network,[22,26] with self-fitting capability for the repairment of massive rotator cuff tear. One of the major advantages of this TIPS technique is its ability to construct macroporous pore networks within the 3D scaffolds,[27] which is highly suitable for BMSCs adhesion and proliferation. The PCL and PEUU scaffolds have been characterized in terms of their physical structure, tensile mechanical properties, and biocompatibility to support the proliferation and migration of rabbit bone mesenchymal stem cells (RBMSCs). Further, considering the ideal biocompatibility of PEUU scaffold, we have investigated its rotator cuff regenerating potential in rabbit model in vivo. To the best of our knowledge, this is the first report of a TIPS-based scaffold that can be useful for repairing massive rotator cuff tears.

2. MATERIALS AND METHODS

2.1. Fabrication of Biomimetic Porous PEUU and PCL Scaffolds by Phase Separation Technique. To prepare the solution for TIPS, we separately dissolved 0.5 g of poly(urethane urea)ester (PEUU, M_w about 80, 000) and 0.5 g of PCL in 10 mL of pure DMSO by placing each solution on a magnetic stirrer at 60 °C for 2 h. After being cast into PTFE molds, the homogeneous solutions were placed in a −80 °C refrigerator for 4 h. The frozen polymers were then subsequently immersed in ice water for 12 h, followed by changing the ice water every 2 h. After being washed with deionized water, the fabricated polymer scaffolds were freeze-dried overnight prior to further experiments.

2.2. Characterization of the PEUU and PCL Scaffold. The morphology of the PCL and PEUU scaffolds was evaluated employing scanning electron microscopy (SEM) (Phenom XL, Netherlands). The pore sizes of the scaffolds were calculated from cross-sectional SEM images using ImageJ software (National Institutes of Health, USA). Fourier transform infrared (FTIR) spectra, water contact angles (WCA), and thermal and mechanical properties of scaffolds were also determined. More characterization details are available in the Supporting Information.

2.3. Cell Proliferation Assay. PEUU and PCL scaffolds were placed into a 100 mm Petri dish and exposed to ultraviolet disinfection for overnight, prior to place them individually into the well of 24-well tissue culture plates. The scaffolds were carefully washed with phosphate buffer solution (PBS) thrice and culture medium once. RBMSCs were seeded at a density of 1.0×10^4 cells/well for cell proliferation assay. The evaluation of the morphology and cell viability of RBMSCs on PEUU and PCL scaffolds (n = 3 for each group) were conducted using SEM and CCK-8 assay following previous studies.[28] To further investigate the morphology of the nucleus and cytoskeleton of proliferated RBMSCs, adhered cells from another set of sheets were fixed with 4% paraformaldehyde and kept at 4 °C prior to further experiments. The nucleus and cytoskeleton of cells were eventually stained with 4′,6′-diamidino-2′-phenylindole hydrochloride (Invitrogen, USA) and rhodamine-conjugated phalloidin (Invitrogen, USA), respectively and observed under Zeiss880 fluorescence microscope (Nikon, Japan).

2.4. Investigation of Cell Migration. The vertical cell migration ability of RBMSCs on both PEUU and PCL scaffolds was investigated (8 μm pores, Corning, USA). After adding 600 μL of α-men with 10% FBS into the lower chambers, the scaffolds (n = 3 for each group) were placed on the upper surface of the membrane. To initiate the migration procedure, we then seeded RBMSCs to the upper chamber (20 000 cells in 300 μL of α-men with 2% FBS). After 12 and 24 h cultivation of cells in an atmosphere of 5% CO_2 and 37 °C temperature, the medium and scaffolds were removed. Cotton tip was used to clean the cells on upper surface of the filter. Migrated RBMSCs on the lower chamber membrane surface were then fixed with 2.5% glutaraldehyde for 15 min at 25 °C. After rinsing thrice with PBS, cells were stained with 300 μL Crystal Violet (Sigma-Aldrich) for 15 min, followed by further washing with PBS twice. To determine the relative migration value, we eluted Crystal Violet staining in 600 μL of 10% acetic acid (30 min, 25 °C) and measured the absorbance at 590 nm.

2.5. Rabbit Rotator Cuff Reconstruction Surgery. The surgical procedures were conducted in rabbit according to the policy of the Institutional Animal Care and Use Committee of Shanghai Jiao Tong University affiliated Shanghai Sixth People's Hospital. The in vivo animal experiments were carried out with approval from the Animal Welfare Ethics Committee of Shanghai Sixth People's Hospital.

Six mature male rabbits of weight 2.5 ± 0.3 kg were used for rotator cuff reconstruction. Both shoulder of these rabbits was shaved carefully and sterilized by iodophor under general anesthesia. The right shoulder of each rabbit was used as experiment group and the left shoulder was served as sham operation group. For experiment group, skin and two layers of deltoid were incised to expose the rotator cuff. Supraspinatus tendons and cartilage on the footprint area were removed using a No. 11 blade knife. The defect was subsequently refilled with PEUU scaffold, fabricated by phase separation technique. After irrigation, the surgical incision was closed. The left shoulder underwent sham surgery, and the deltoid and skin were closed in a routine manner, without any damage on rotator cuff. After recovering from anesthesia, all animals were allowed to move unrestrictedly inside the cage. Three days postsurgery, 400 000 U of penicillin was administered to the muscle to prevent infection. Three months postsurgery, 12 rotator cuff tendon-humerus complexes were harvested for histological study and biomechanical testing. Micro-CT, histological, histochemical, and biomechanical assessments of rotator cuff for both the experimental group as well as sham operation group

https://dx.doi.org/10.1021/acsbiomaterials.0c00193
ACS Biomater. Sci. Eng. 2021, 7, 904−915

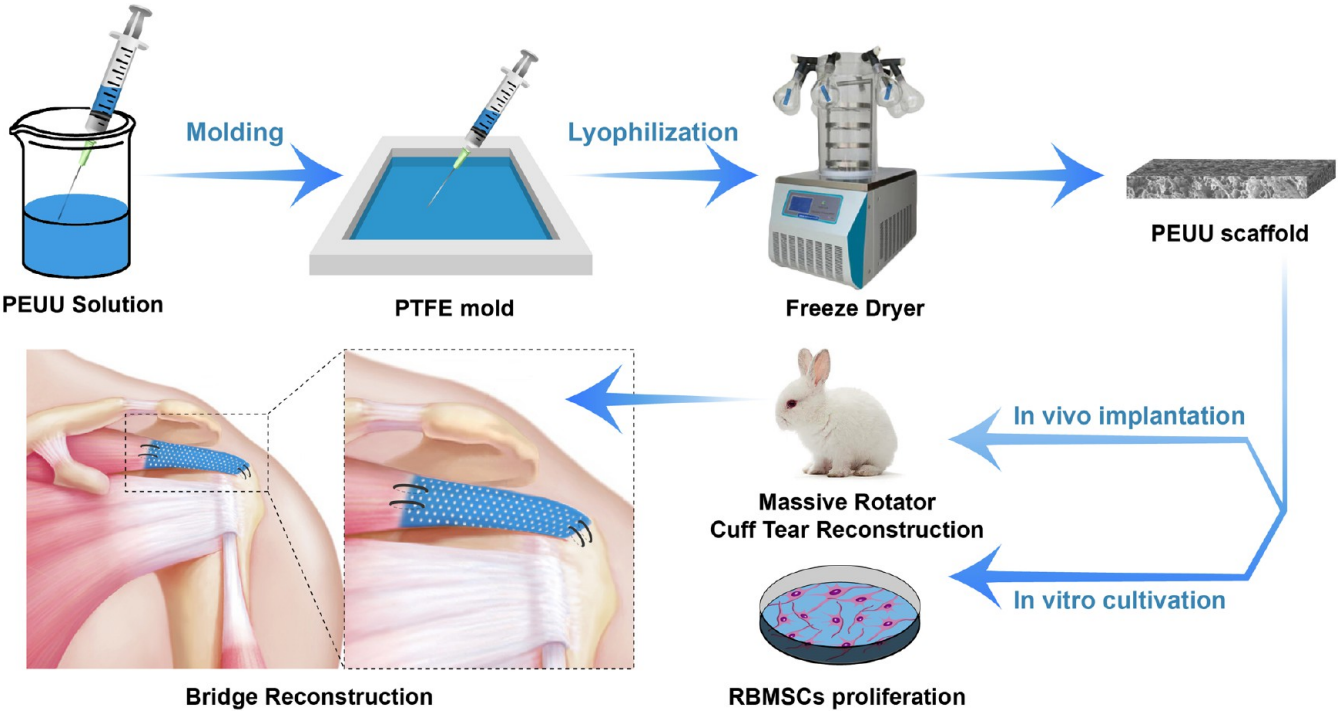

Figure 1. Schematic illustrations of fabrication of PEUU macroporous 3D scaffold and its therapeutic application for massive rotator cuff defect in vitro and in vivo.

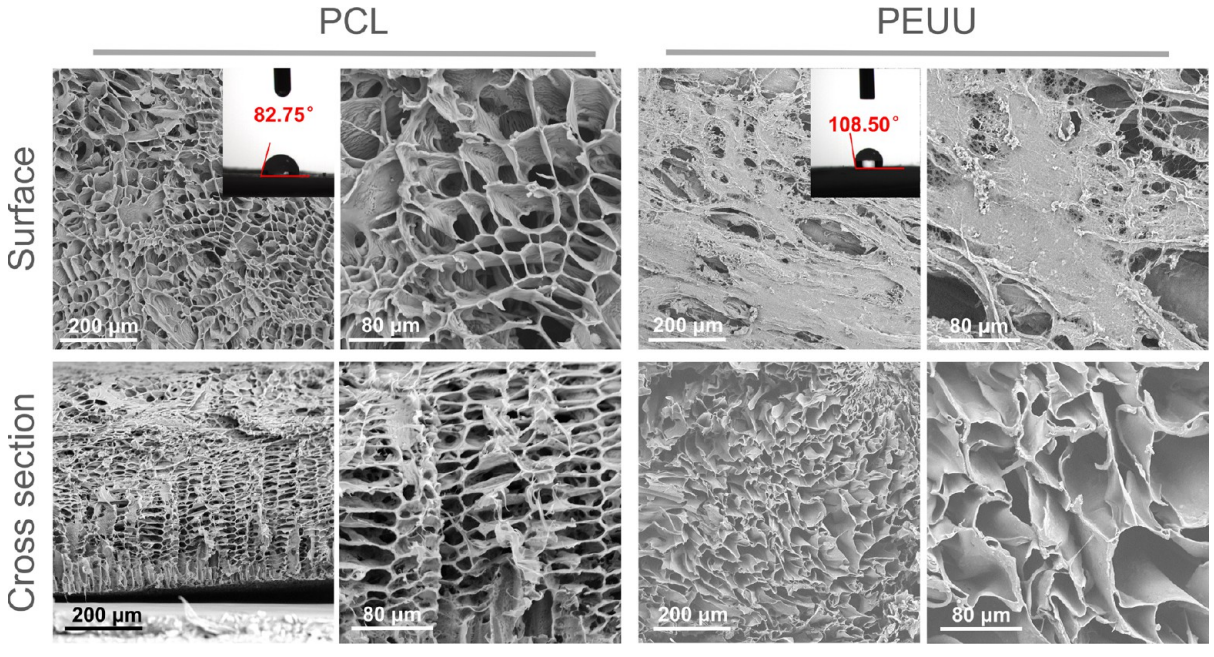

Figure 2. SEM images exhibiting cross-sectional and surface structure of PCL and PEUU scaffolds and measurement of their water contact angle (images of drops captured at 0.5 s), respectively.

were performed. More testing details are available in the Supporting Information.

2.6. Statistical Analysis. All quantitative data were presented as the mean ± standard error. All statistical analyses were performed employing independent-Sample *t* test and significant level was set at $P < 0.05$.

3. RESULTS

3.1. Fabrication and Characterization of Scaffolds. According to the previous reports, the smaller pore size of the scaffold may hamper the infiltration of host cells as well as limit the regeneration and remodeling of the tissue.[29] Therefore, in the current study, we decided to design a macroporous 3D scaffold for rapid and effective regeneration of massive rotator cuff defect. An earlier study reported that the enhanced level of porosity in the microstructure of the scaffold is commonly accompanied by the reduction of mechanical strength originating from large void space.[8] In this context, we have designed a sheet 3D scaffold with an oriented macroporous structure. The fabrication of scaffold was carried out by

https://dx.doi.org/10.1021/acsbiomaterials.0c00193
ACS Biomater. Sci. Eng. 2021, 7, 904−915

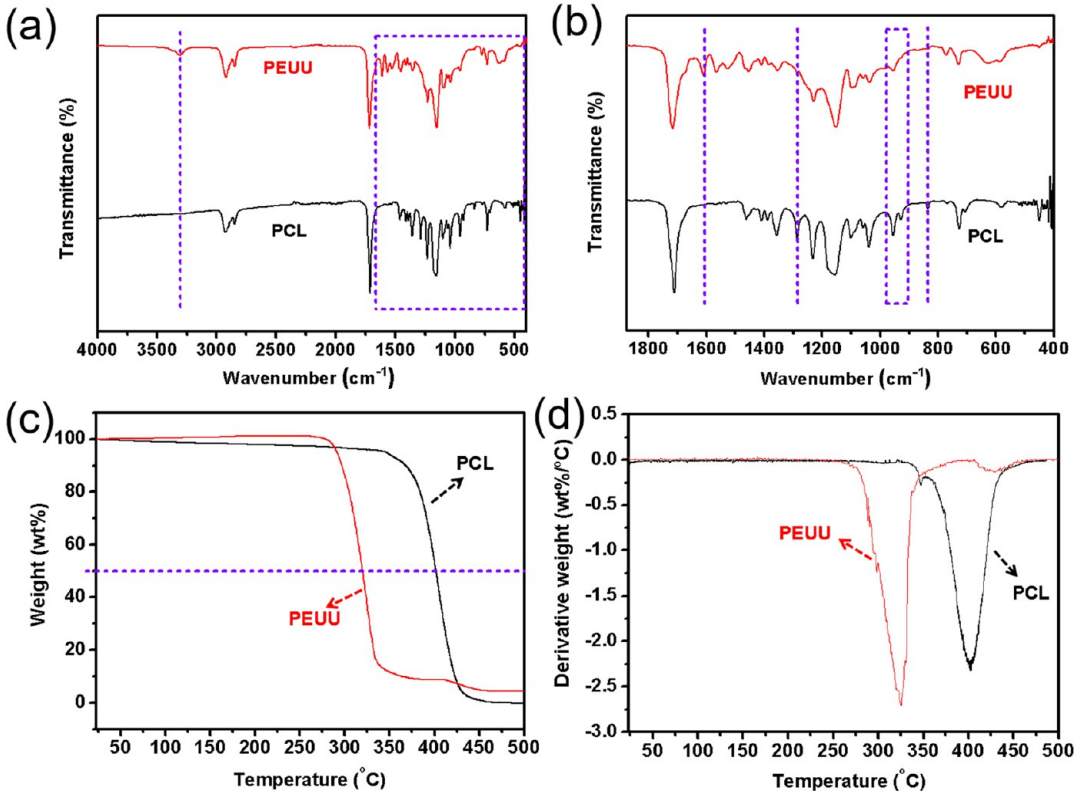

Figure 3. (a, b) FTIR spectra curves of PCL and PEUU scaffolds. (a) 400−4000 cm^{-1} wavenumber range; (b) 400−1875 cm^{-1} wavenumber range; (c, d) TG and DTG curves of PCL and PEUU scaffolds.

pouring 5% PEUU homogeneous solutions into the PTFE molds, followed by freeze-drying treatment (as depicted in Figure 1).

It is highly essential to characterize the microstructure of the scaffold, as the three-dimensional structure of the as-prepared scaffold may easily be damaged during TIPS operation. The structure of the outside and cross-sectional surface as well as surface wettability of both PCL and PEUU scaffolds were determined by SEM analysis and water contact angle measurement, respectively, as shown in Figure 2. It is clearly observed from SEM images that the synthesized PEUU scaffold possess a microporous fluffy outer surface, whereas PCL scaffold exhibited a macroporous ordered outer surface. The fluffy compact outer surface of PEUU scaffold would provide a suitable architecture for the adhesion and proliferation of RBMSCs. The water contact angles of the outer surface of the two scaffolds indicate that the pore structures determine their hydrophilicity, which might result in different biocompatibility.

The pore structures of PCL and PEUU scaffolds exhibited different morphological properties as observed from cross-sectional SEM images. PCL scaffold showed a flap and irregular pore structure, which might restrict the cell migration. However, PEUU scaffold displayed a regular and interconnected structure with a pore size of about 40−80 μm, which is highly suitable for cell migration. Moreover, the prepared PEUU scaffold is macroscopically smooth without any gross defects and the structures of the tube remain intact after the TIPS operation, indicating that the TIPS process results in no visible changes in the morphology of the scaffold.

Via a two-step solution polymerization method, the PEUU scaffold was synthesized following our previous work.[28] As shown in Figure 3a,b, FTIR spectroscopy was used to confirm the different chemical structures of PCL and PEUU scaffolds. The intensity of the infrared vibration absorption peak is proportionally related to the polarity of the bond. The stronger the polarity, the higher is the intensity. Therefore, the peak intensity of C═O is generally higher than that of C═C. The spectrum presented characteristic peaks of PEUU at around 3300 cm^{-1} (C−H vibrations on unsaturated C), 1600 cm^{-1} (stretching vibration), 1725 cm^{-1} (ester carbonyl group), and 1570 cm^{-1} (the deformation vibration in plane of N−H). The broad peaks of PEUU were at 1161 and 1280 cm^{-1}, representing the stretching vibration of C−O−C. The vibration of the C−O stretching and C−N stretching exhibited peaks at 1088 and 1454 cm^{-1}, respectively.

The stability of the scaffolds was determined by thermogravimetric analysis as recommended.[30] Thermogravimetric (TG) and differential thermogravimetric (DTG) curves of PCL and PEUU scaffolds are presented in Figure 3c, d, respectively. The thermal degradation temperature of the PCL scaffold is in the range of 300−500 °C and the temperature of 50% weight loss is near 410 °C. Two stages of pyrolytic process were observed for PEUU scaffold, unlike one-stage pyrolytic process of PCL scaffold. The first stage represents the thermal fracture of soft segment of main molecular chains and the second stage can be ascribed to the thermal scission of hard segment of main molecular chains. Furthermore, the thermal degradation temperature of 50% weight loss of PEUU scaffold was decreased slightly. As shown in Figure 3d, the weight of PEUU scaffold was reduced greatly from approximately 250 to 500 °C, which is significantly less than that of PCL scaffold. Therefore, the result demonstrated that PEUU is a block

https://dx.doi.org/10.1021/acsbiomaterials.0c00193
ACS Biomater. Sci. Eng. 2021, 7, 904−915

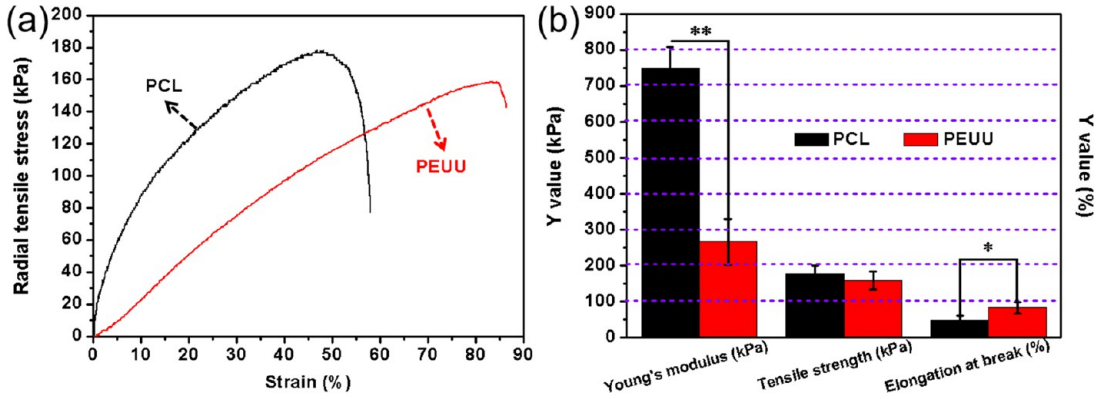

Figure 4. Mechanical properties of PCL and PEUU scaffolds under dry conditions. (a) representative stress−strain curves; (b) Young's modulus, tensile strength, and elongation at break. *P < 0.05, **P < 0.01.

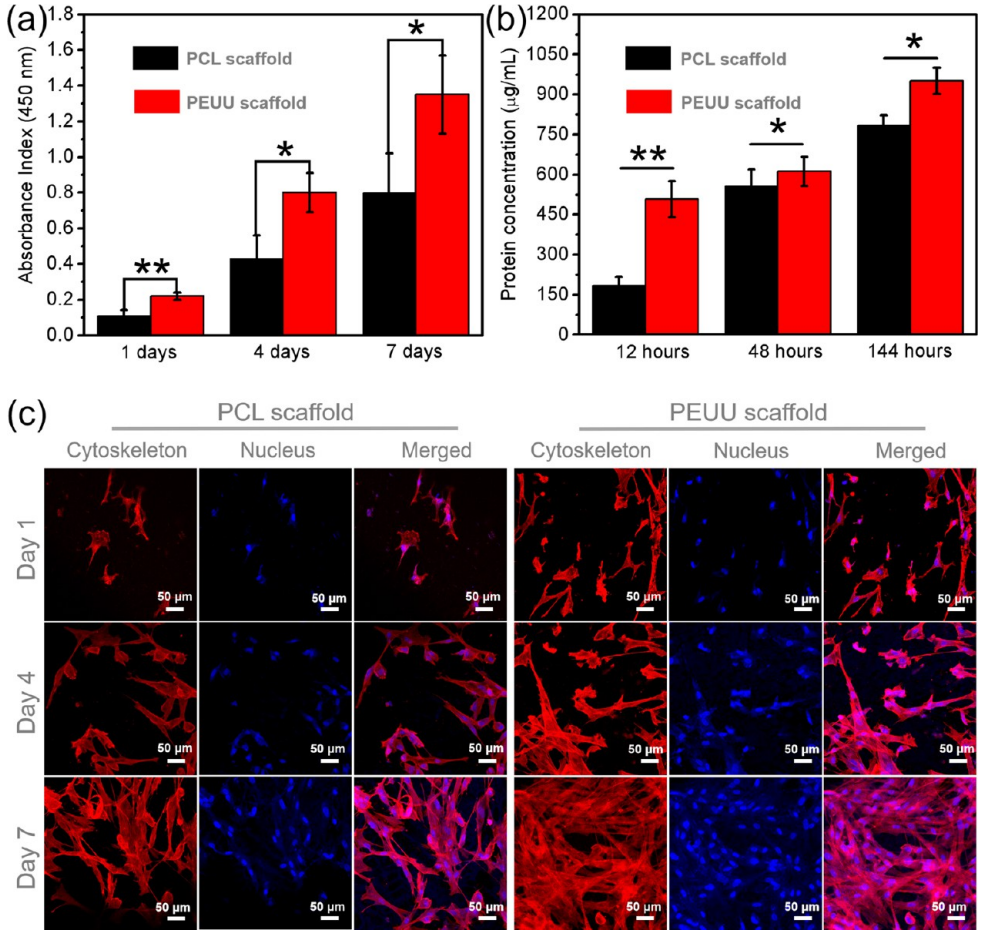

Figure 5. Biocompatibility of PCL and PEUU scaffolds. (a) CCK-8 assay for the viability of RBMSCs cultured onto PCL and PEUU scaffolds for 1, 4, and 7 days, respectively. (b) Protein absorption results of PCL and PEUU scaffolds for 12, 48, and 144 h, respectively. (c) DAPI (blue)/phalloidin (red) staining of RBMSCs proliferation. Scar bar: 50 μm. The results are shown as mean ± standard deviation. *P < 0.05, **P < 0.01.

polymer, which is more likely to induce the separation of two phases.

3.2. Mechanical Properties. Representative stress−strain curves, Young's modulus, tensile strength, and elongation at break of PCL and PEUU scaffolds are presented in Figure 4a, b, respectively. In comparison with PCL scaffold, the macroporous structure of PEUU scaffold leads to an obvious decrease in Young's modulus and an evident increase in elongation at break of the scaffold in dry conditions.

3.3. Cytocompatibility Assay. It is highly critical to ensure the biocompatibility of the developed scaffold prior to its biomedical application. The proliferation of RBMSCs seeded on scaffold after 1, 4, and 7 days of culture is presented in Figure 5. The morphology of RBMSCs cultured onto the PCL and PEUU scaffold was observed after incubation by rhodamine-conjugated phalloidin/DAPI staining under fluorescence microscopy. As is shown in Figure 5c, the density of RBMSCs cultured on PEUU scaffold were higher than PCL scaffold. The absorbance index of RBMSCs cultured on PCL

https://dx.doi.org/10.1021/acsbiomaterials.0c00193
ACS Biomater. Sci. Eng. 2021, 7, 904−915

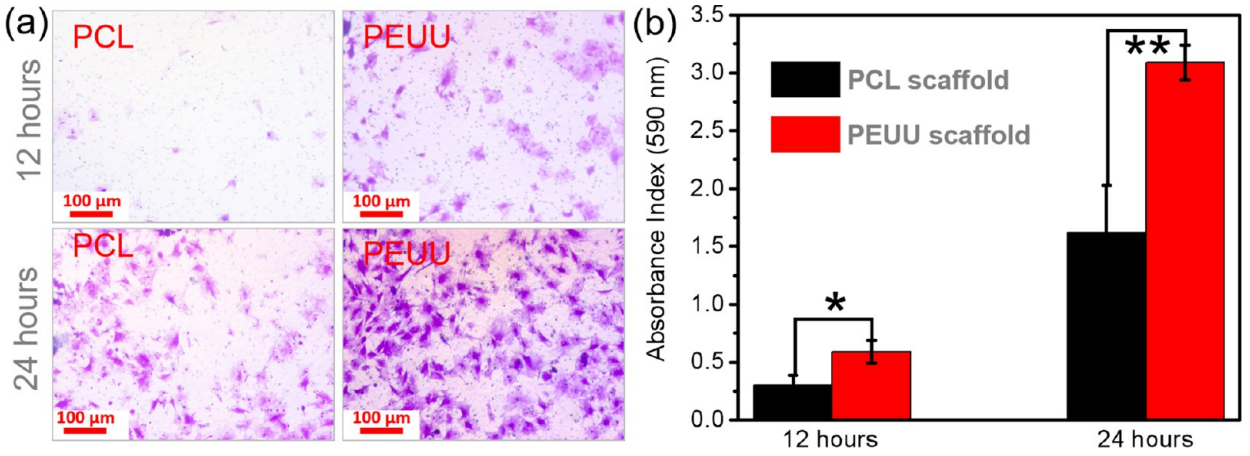

Figure 6. RBMSCs vertical migration ability. (a) Representative images of RBMSCs located on the lower site of the transwell assay after migration through the PCL or PEUU scaffold; (b) quantification of the relative RBMSCs migration in the two scaffolds. Scar bar: 100 μm. The results are shown as mean ± standard deviation. *P < 0.05, **P < 0.01.

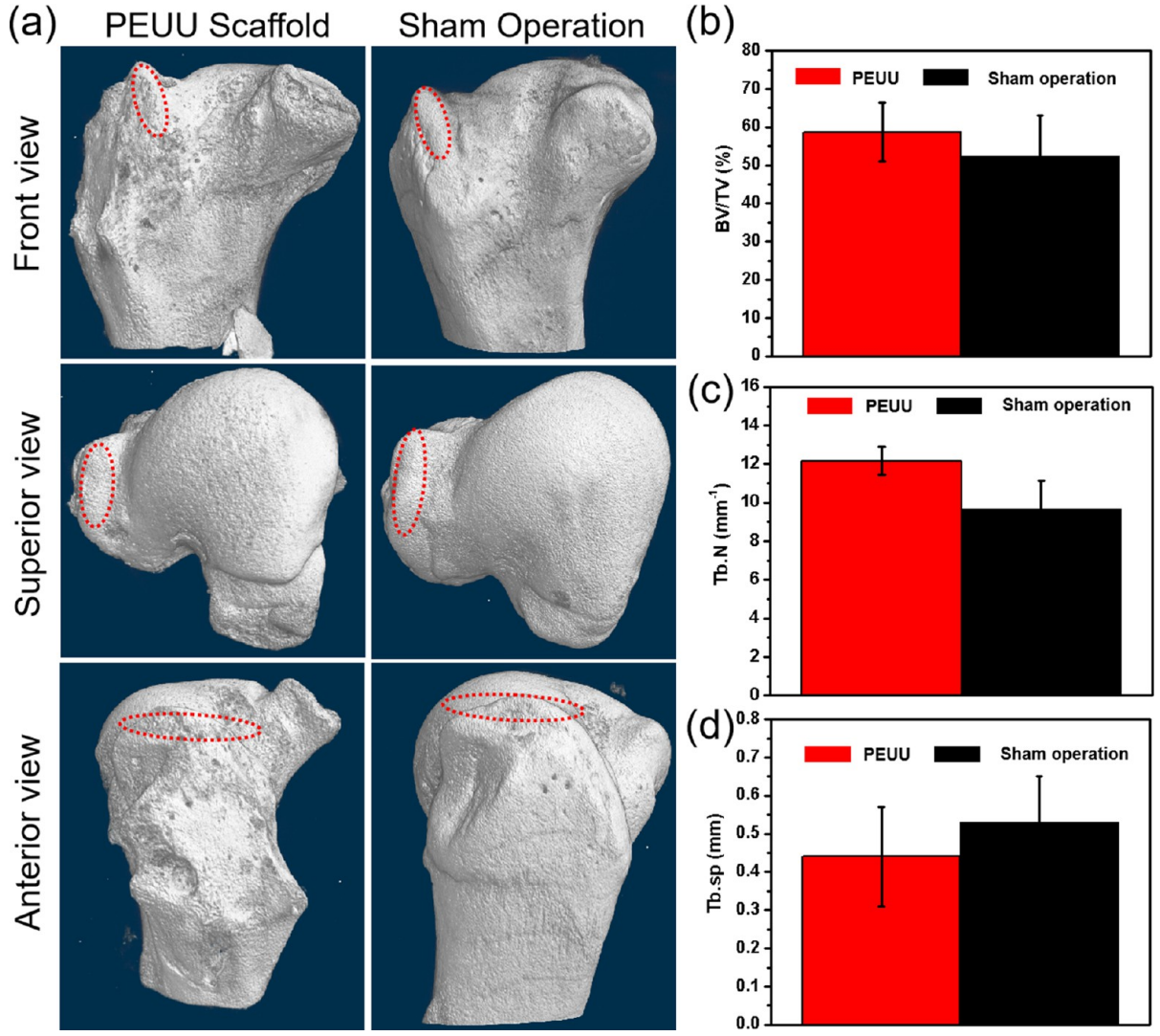

Figure 7. Representative microcomputed tomography images of the proximal humerus and quantitive analysis. (a) Red oval indicate newly formed bone between supraspinatus tendon and bone; Quantitive analysis of (b) BV/TV, (c) Tb.N, and (d) Tb.sp. BV/TV, bone volume/total volume; Tb.sp, trabecular separation; Tb.N, trabecular number.

scaffold is 0.11 ± 0.03, 0.43 ± 0.13, and 0.80 ± 0.22 on 1, 4, and 7 days, respectively as shown in Figure 5a. As compared to PCL scaffold, PEUU was much more suitable for proliferation of RBMSCs and absorbance index of RBMSCs cultured on

https://dx.doi.org/10.1021/acsbiomaterials.0c00193
ACS Biomater. Sci. Eng. 2021, 7, 904−915

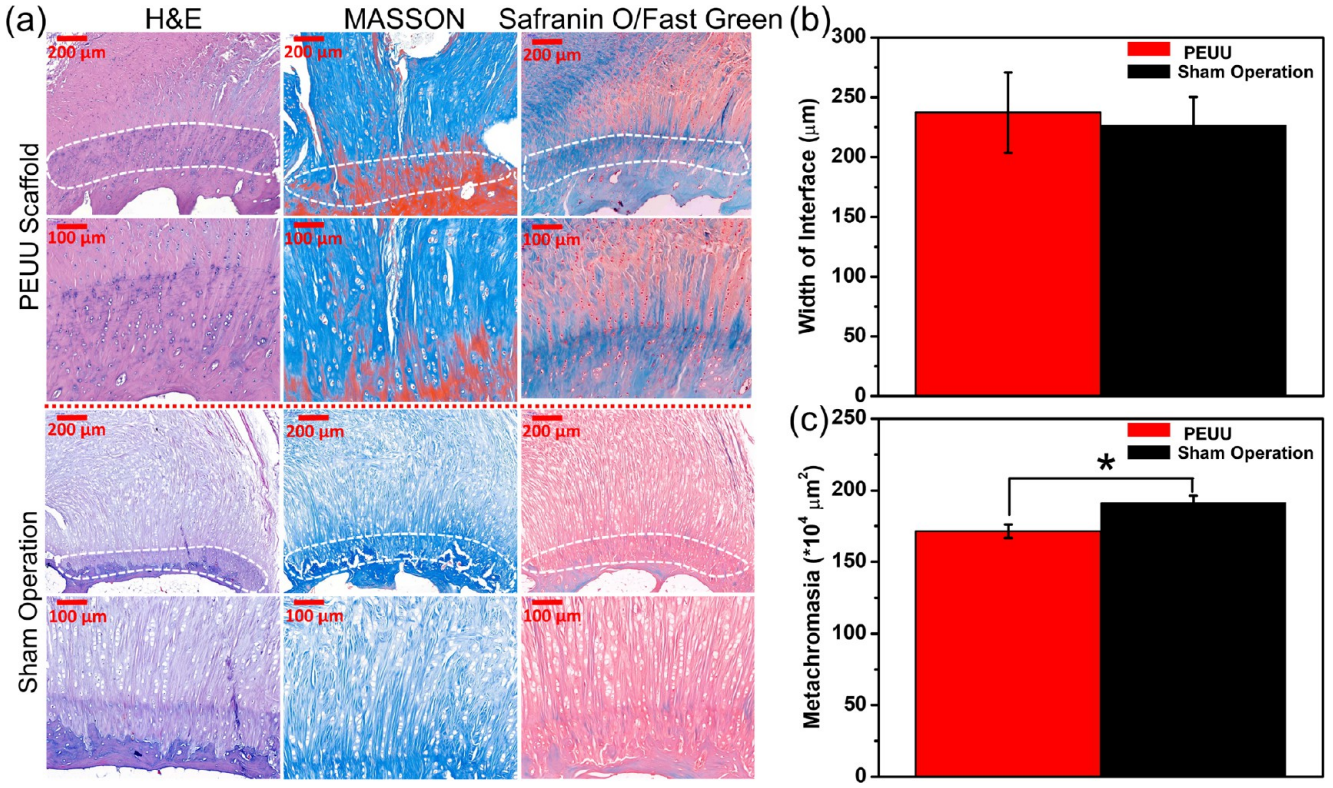

Figure 8. Postsurgery representative images of tendon-bone interface regeneration and quantitive analysis. (a) HE, MASSON and Saafranin O/Fast Green staining images; (b, c) quantitative analysis of regeneration. The interface is outlined by the white line. $^*P < 0.05$.

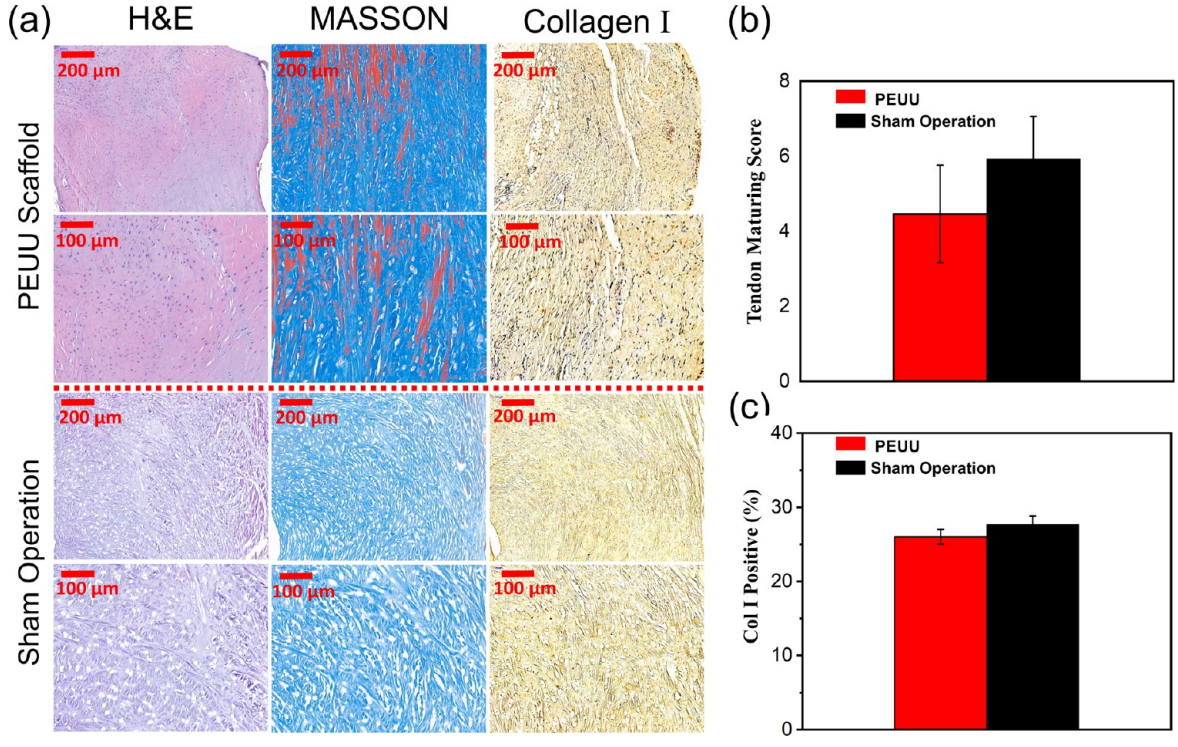

Figure 9. Postsurgery representative images of tendon regeneration and quantitive analysis. (a) HE, MASSON and immunochemical Collagen I staining images at three months; (b, c) quantitative analysis of regeneration.

PEUU scaffold is 0.22 ± 0.02, 0.80 ± 0.11, and 1.35 ± 0.22 on 1, 4, and 7 days, respectively. Significant differences of absorbance index were observed on all the observation time points for these two scaffolds. It is well-known that protein plays an important role in cell survival and adhesion. The protein adsorption of the two scaffolds was increased with time as shown in Figure 5b. As compared to PCL scaffold, PEUU scaffold was able to absorb more protein at a particular time

https://dx.doi.org/10.1021/acsbiomaterials.0c00193
ACS Biomater. Sci. Eng. 2021, 7, 904−915

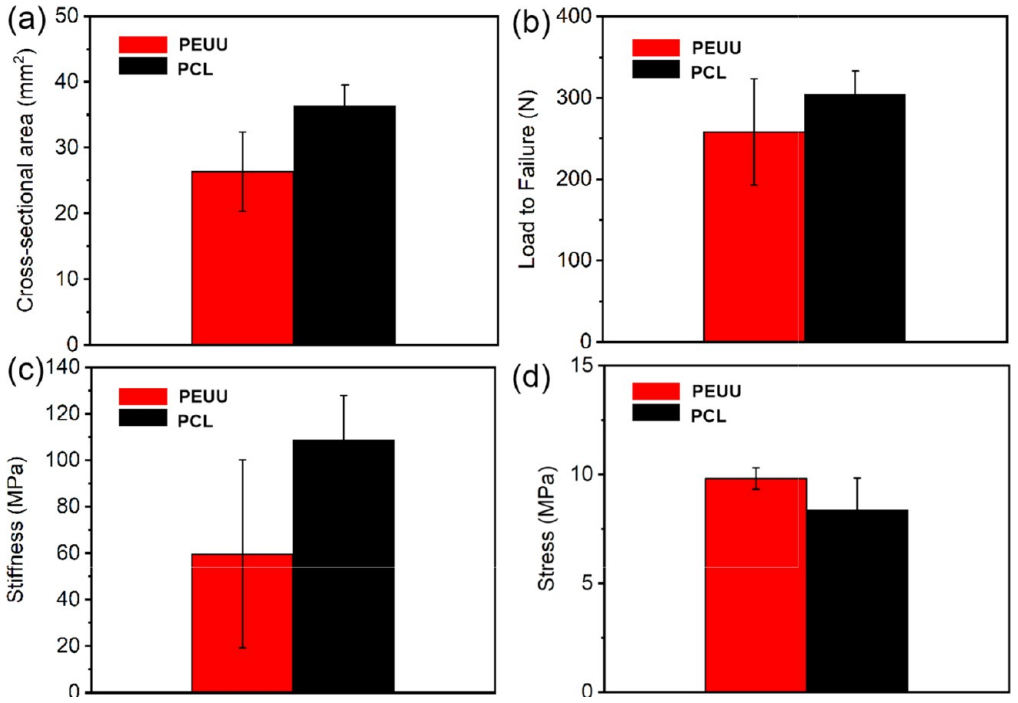

Figure 10. Biomechanical testing of the tendon at the insertion site. (a) Cross-sectional areas, (b) load to failure, (c) stiffness, and (d) ultimate stress to failure values. The results are shown as mean ± standard deviation.

point, indicating that PEUU scaffold possess stronger sustained protein absorption ability. As shown in Figure 2, the PEUU scaffold exhibited microporous fluffy outer surface, whereas the PCL scaffold possess macroporous ordered outer surface, which might be due to the fact that PEUU is more likely to absorb the protein inside of scaffold, whereas the proteins are mostly located on the surface of PCL scaffolds, during long-term contact with protein.

3.4. Cell Migration. The biological process of rotator cuff regeneration involves the migration of RBMSCs. Therefore, the ability of PEUU and PCL scaffolds to induce directional motility of RBMSCs was evaluated as shown in Figure 6. The absorbance index of RBMSCs seeded on PCL scaffold is 0.30 ± 0.09 after 12 h of migration and the index of RBMSCs seeded on PEUU scaffold was increased up to 0.59 ± 0.10 ($P < 0.05$). After 24 h of migration, the absorbance index was greatly elevated. The absorbance index of BMSCs seeded on PCL scaffold was 1.62 ± 0.41 and index of BMSCs seeded on PEUU scaffold was increased up to 3.09 ± 0.15 ($P < 0.05$).

3.5. Macroscopic Observations. No evident infection at the surgical site was grossly observed in any experimental rabbit. No remnants of PEUU scaffolds were observed and the continuity of damaged rotator cuff were fully recovered. The peritendinous fibrosis reaction was spotted in each complex. No remnant of implant was observed at the tendon attachment site footprint.

3.6. Micro-CT Analysis. The subchondral bone in the experiment group exhibited no remarkable loss of bone volume and degeneration of the trabecular bone structure, as observed from the micro-CT evaluation (Figure 7). Evaluation of the BV/TV in experiment group is 58.71 ± 7.76% and there was no significant differences as compared to the sham operation group 52.45 ± 10.64% ($P = 0.457$). Additionally, Tb.N (12.15 ± 0.72 mm^{-1}) for experiment group was also not significantly different as compared to the sham operation group (9.67 ± 1.45 mm^{-1}, $P = 0.057$). Evaluation of Tb.sp also showed no significant difference between experiment group (0.44 ± 0.13 mm) and sham operation group (0.53 ± 0.12 mm, $P = 0.411$).

3.7. Histological Analysis. The histological analysis exhibited a successful regeneration of tendon−bone interface employing PEUU scaffold and no remnant of scaffold was observed (Figure 8). Marked by a grid, the width of the interface that had been fully destroyed during the surgery in the experiment group, was fully regenerated. The widths of interface of experiment group and sham operation group are 237.30 ± 33.66 μm and 226.60 ± 23.74 μm ($P = 0.676$), respectively. However, the metachromasia value of tendon-to-bone interface in experiment group (171.38 ± 4.76) was significantly different as compared to the normal tendon (191.17 ± 4.76, $P = 0.003$).

For tendon regeneration, the tendon defect was replaced by well-oriented collagen fibers. Tendon maturing score of experiment group and sham operation group were observed with no significant differences in the respective scores of 26.00 ± 1.00 and 27.70 ± 0.58 ($P = 0.067$) as shown in Figure 9. The evaluation of collagen I positive cells demonstrated no significant difference between experiment group (4.46 ± 1.30%) and sham operation group (5.93 ± 1.13%, $P = 0.21$). However, the area of metachromasia value of tendon tissue in experiment group (139.21 ± 4.68) was significantly different in comparison with the normal tendon (191.47 ± 10.84, $P = 0.002$).

3.8. Biomechanical Testing. All the sample failed at the middle of tendon in the biomechanical testing. The load to failure score in the experiment group (258.00 ± 65.37 N) was a little bit lower than that of the sham operation group (304.67 ± 28.29 N), but there was no significant difference ($P = 0.32$) between them as shown in Figure 10. Stiffness evaluation also exhibited no significant difference between experiment group (59.67 ± 40.50 MPa) and sham operation group (108.67 ± 19.14 MPa, $P = 0.131$). The stress in the experiment group (9.82 ± 0.49 MPa) was a little bit higher than that of the sham

https://dx.doi.org/10.1021/acsbiomaterials.0c00193
ACS Biomater. Sci. Eng. 2021, 7, 904−915

operation group (8.38 ± 1.46 MPa), but there was no significant difference as well (P = 0.18). Cross-sectional area assessment also depicted no significant difference between experiment group (26.33 ± 6.02 mm^2) and sham operation group (36.33 ± 3.21 mm^2, P = 0.064).

4. DISCUSSION

During old age, massive rotator cuff defects are one of the most common pathological conditions, and direct repair is impossible because of chronicity and defect size.[31−33] Various methods have been developed to address the challenges associated with massive rotator cuff tear. Among these methods, structural amendment with biological scaffolds is the most direct and convenient option.[34,35] However, the substitutes must fully transform to autologous physiological tissues for successful regeneration. In this regard, the biocompatibility, favorable porosity, and mechanical property of biological scaffolds are highly critical.[36,37]

The scaffolds designed for massive rotator cuff defect repair should not only induce the tendon regeneration but should also induce physical tendon-to-bone interface regeneration.[27,38] Considering the rotator cuff is a relative avascular structure, the regeneration induced by scaffold is much more difficult. The earlier studies have mainly concentrated on regeneration of the tendon-to-bone interface.[39] Instead of total removal of supraspinatus and cartilage on the footprint, they simply split the supraspinatus tendon from its footprint. Then an electrospinning fibrous membrane mixed with growth factors/cytokines was added between the tendon and bone and the remnant tendon was sutured in situ. However, this strategy is far from practical clinical condition. Remnant tendon of massive rotator cuff defect usually causes atrophies, and direct suture would result in severe tendon degeneration even in the presence of a regeneration induction membrane due to excessive loading.[40,41] Thus, a scaffold, rather than a membrane, that can bridge the remnant tendon and its footprint on the bone matches the clinical needs.

Highly porous scaffolds can be prepared through the TIPS procedure, which is critical for tissue regeneration.[42,43] Though no consensus regarding the certain porosity values, ideal pore size, and percentage of interconnected pores has been made, previous reports confirmed that high porosity values are advantageous for tissue regeneration. The present study revealed that the scaffold prepared through the TIPS procedure not only supports adhesion and proliferation of RBMSCs but also facilitates their immigration.

Different synthetic polymers have widely been investigated for tissue engineering applications. Among them, PCL is one of the representative biodegradable polymer materials with excellent biocompatibility and good mechanical properties. Recently, extensive electrospinning studies have been conducted to fabricate PCL-based hybrid nanofibrous scaffolds with desirable mechanical properties for ameliorating rotator cuff damage. Until now, little study has been reported for the preparation of mechanically matched PCL-based composite scaffold via TIPS technique for regeneration of rotator cuff tissue. PCL is a hemicrystalline polymer that forms the irregular structure via TIPS method, limiting the adequate infiltration of cells. Contrastingly, PEUU is an elastomeric biodegradable polymer, developed recently from PCL low-molecular-weight diol, for tissue engineering applications exploiting its tunable mechanical properties. This PEUU scaffold is processable into grafts easily through thermally induced phase separation. In the present study, we have confirmed that the PCL scaffold synthesized via TIPS method had smaller water contact angle, as compared to that of PEUU scaffold. We have hypothesized that the water contact angle difference originates from the macrostructural features of fabricated scaffolds, which have been confirmed to influence cell survival and growth, as well as playing a critical role in modulating cell phenotype and functions.[44] In the current study, we found that fluffy compact outer surface and interconnected structure of PEUU scaffold fabricated via TIPS is much more suitable for cell proliferation and migration, as compared to that of PCL scaffold. As illustrated by earlier literature, the promotion of BMSCs proliferation is critical for tendon-to-bone regeneration.[45,46] We have also observed that proliferated and migrated RBMSCs may play an essential role in the successful rotator cuff regeneration in vivo.

For MRCT reconstruction, the critical issue of scaffold is to endure the tension of daily activity, after in situ implantation. Thus, mechanical property of scaffold is highly important in this regard.[47,48] However, the materials with improved mechanical properties might limit the growth of host cells. Foyt DA et. al suggested that soft scaffold can better support cell proliferation and cartilage regeneration as compared to stiff scaffold.[49] Thus, soft scaffold which would not break during degeneration, could be suitable for rotator cuff regeneration. In the current study, we have revealed that compared to the PCL scaffold, the biocompatibility and mechanical property of PEUU scaffold was much suitable for rotator cuff regeneration. We have hypothesized that as compared to the PCL scaffold possessing only a soft segment, the hard segment of the PEUU scaffold not only strengthens its mechanical property but also offers better structure for cell proliferation. As suggested by earlier study, PEUU scaffold may also be of interest for soft tissue engineering, including tendon reconstruction or vascular tissue engineering.[50] However, whether it can successfully induce tendon-to-bone regeneration was remained uncertain. In this study, we confirmed through histological analysis that tendon-to-bone interface was regenerated employing PEUU scaffold. It is hypothesized that because the PEUU scaffold has a long degeneration time, there are enough time for BMSCs to infiltrate and proliferate without interruption.[50] Moreover, the mechanical stimulation is one of the key factors of tendon-to-bone regeneration in vivo.[51] All these factors would contribute to the successful regeneration of rotator cuff.

5. CONCLUSION

In summary, we successfully fabricated a macroporous 3D PEUU scaffold with self-fitting capability by TIPS method for massive rotator cuff tear regeneration. In vitro studies suggested that PEUU scaffold could better support the proliferation and migration of RBMSCs. Further, in vivo studies confirmed that the PEUU scaffold can efficiently induce physical tendon-to-bone and tendon regeneration in a rabbit model of massive rotator cuff tear. Micro-CT evaluation suggested that BV/TV in PEUU scaffold induced regenerative tissue is 58.71% ± 7.76%, with no significant differences as compared to normal rotator cuff. Additionally, biomechanical studies exhibited that load to failure in experiment group is 258.00 N ± 65.37 N, which is also similar to the normal rotator cuff, with no significant difference. This plerosis function of the scaffold most likely resulted from its porous structure. Therefore, the PEUU scaffold with macroporous 3D structure can be employed for the development of biodegrad-

https://dx.doi.org/10.1021/acsbiomaterials.0c00193
ACS Biomater. Sci. Eng. 2021, 7, 904−915

able composite rotator cuff grafts for repairing a massive rotator cuff tear.

■ ASSOCIATED CONTENT

Supporting Information

The Supporting Information is available free of charge at https://pubs.acs.org/doi/10.1021/acsbiomaterials.0c00193.

Detailed experimental section for materials, characterization of the PEUU and PCL scaffold, micro-CT analysis, histological and histochemical analysis, and biomechanical testing (PDF)

■ AUTHOR INFORMATION

Corresponding Authors

Jinzhong Zhao − *Department of Sports Medicine, Department of Orthopedics, Shanghai Jiao Tong University Affiliated Sixth People's Hospital, Shanghai 200233, PR China;* orcid.org/0000-0003-2265-1878; Phone: +86 21 24056088; Email: jzzhao@sjtu.edu.cn; Fax: +86 21 24056088

Tonghe Zhu − *Department of Sports Medicine, Department of Orthopedics, Shanghai Jiao Tong University Affiliated Sixth People's Hospital, Shanghai 200233, PR China;* Email: zhutonghe@sjtu.edu.cn

Authors

Liren Wang − *Department of Sports Medicine, Department of Orthopedics, Shanghai Jiao Tong University Affiliated Sixth People's Hospital, Shanghai 200233, PR China*

Yuhao Kang − *Department of Sports Medicine, Department of Orthopedics, Shanghai Jiao Tong University Affiliated Sixth People's Hospital, Shanghai 200233, PR China*

Sihao Chen − *Multidisciplinary Center for Advanced Materials, Advanced Research Institute, Shanghai University of Engineering Science, Shanghai 201620, PR China*

Xiumei Mo − *State Key Laboratory for Modification of Chemical Fibers and Polymer Materials, College of Chemistry, Chemical Engineering and Biotechnology, Donghua University, Shanghai 201620, PR China;* orcid.org/0000-0001-9238-6171

Jia Jiang − *Department of Sports Medicine, Department of Orthopedics, Shanghai Jiao Tong University Affiliated Sixth People's Hospital, Shanghai 200233, PR China*

Xiaoyu Yan − *Department of Sports Medicine, Department of Orthopedics, Shanghai Jiao Tong University Affiliated Sixth People's Hospital, Shanghai 200233, PR China*

Complete contact information is available at: https://pubs.acs.org/10.1021/acsbiomaterials.0c00193

Funding

This work was supported by China Postdoctoral Science Foundation [Grant 2019M661525], National Natural Science Foundation of China [Grant 81902186, 81671920, 31972923, 81871753, and 81772341], National Key Research and Development Program of China [Grant 2018YFC1106200, 2018YFC1106201, 2018YFC1106202], and Technology Support Project of Science and Technology Commission of Shanghai Municipality of China [Grant 19441901700, 19441901701, 19441902702, and 18441902800].

Notes

The authors declare no competing financial interest.

■ ACKNOWLEDGMENTS

The authors declare no competing financial interest.

■ REFERENCES

(1) Camurcu, Y.; Ucpunar, H.; Ari, H.; Duman, S.; Cobden, A.; Sofu, H. Predictors of allocation to surgery in patients older than 50 years with partial-thickness rotator cuff tear. *J. Shoulder Elbow Surg* **2019**, *28*, 828−832.

(2) Shim, S. B.; Jeong, J. Y.; Kim, J. S.; Yoo, J. C. Evaluation of risk factors for irreparable rotator cuff tear in patients older than age 70 including evaluation of radiologic factors of the shoulder. *J. Shoulder Elbow Surg* **2018**, *27*, 1932−1938.

(3) Shim, S. B.; Jeong, J. Y.; Yum, T. H.; Yoo, J. C. A Comparative Study to Evaluate the Risk Factors for Medium-Sized Rotator Cuff Tear in Patients Younger Than 50 Years of Age. *Arthroscopy* **2018**, *34*, 2971−2979.

(4) Chen, K. H.; Chiang, E. R.; Wang, H. Y.; Ma, H. L. Arthroscopic Partial Repair of Irreparable Rotator Cuff Tears: Factors Related to Greater Degree of Clinical Improvement at 2 Years of Follow-Up. *Arthroscopy* **2017**, *33*, 1949−1955.

(5) Seker, V.; Hackett, L.; Lam, P. H.; Murrell, G. A. C. Evaluating the Outcomes of Rotator Cuff Repairs With Polytetrafluoroethylene Patches for Massive and Irreparable Rotator Cuff Tears With a Minimum 2-Year Follow-up. *Am. J. Sports Med.* **2018**, *46*, 3155−3164.

(6) Orr, S. B.; Chainani, A.; Hippensteel, K. J.; Kishan, A.; Gilchrist, C.; Garrigues, N. W.; Ruch, D. S.; Guilak, F.; Little, D. Aligned multilayered electrospun scaffolds for rotator cuff tendon tissue engineering. *Acta Biomater.* **2015**, *24*, 117−26.

(7) Novakova, S. S.; Mahalingam, V. D.; Florida, S. E.; Mendias, C. L.; Allen, A.; Arruda, E. M.; Bedi, A.; Larkin, L. M. Tissue-engineered tendon constructs for rotator cuff repair in sheep. *J. Orthop. Res.* **2017**, *36*, 289−299.

(8) Saveh-Shemshaki, N.; Nair, L. S.; Laurencin, C. T. Nanofiber-based matrices for rotator cuff regenerative engineering. *Acta Biomater.* **2019**, *94*, 64−81.

(9) Sun, Y. Y.; Han, F.; Zhang, P.; Zhi, Y. L.; Yang, J. J.; Yao, X. H.; Wang, H.; Lin, C.; Wen, X.; Chen, J. W.; Zhao, P. A synthetic bridging patch of modified co-electrospun dual nano-scaffolds for massive rotator cuff tear. *J. Mater. Chem. B* **2016**, *4*, 7259−7269.

(10) Willbold, E.; Wellmann, M.; Welke, B.; Angrisani, N.; Gniesmer, S.; Kampmann, A.; Hoffmann, A.; de Cassan, D.; Menzel, H.; Hoheisel, A. L.; Glasmacher, B.; Reifenrath, J. Possibilities and limitations of electrospun chitosan-coated polycaprolactone grafts for rotator cuff tear repair. *J. Tissue Eng. Regener. Med.* **2020**, *14*, 186−197.

(11) Orr, S. B.; Chainani, A.; Hippensteel, K. J.; Kishan, A.; Gilchrist, C.; Garrigues, N. W.; Ruch, D. S.; Guilak, F.; Little, D. Aligned multilayered electrospun scaffolds for rotator cuff tendon tissue engineering. *Acta Biomater.* **2015**, *24*, 117−126.

(12) Zhao, S.; Zhao, X.; Dong, S. K.; Yu, J.; Pan, G. Q.; Zhang, Y.; Zhao, J. Z.; Cui, W. G. A hierarchical, stretchable and stiff fibrous biotemplate engineered using stagger-electrospinning for augmentation of rotator cuff tendon-healing. *J. Mater. Chem. B* **2015**, *3*, 990−1000.

(13) Zhao, Y. D.; Tan, K.; Zhou, Y.; Ye, Z. Y.; Tan, W. S. A combinatorial variation in surface chemistry and pore size of three-dimensional porous poly(epsilon-caprolactone) scaffolds modulates the behaviors of mesenchymal stem cells. *Mater. Sci. Eng., C* **2016**, *59*, 193−202.

(14) Zhang, Y. F.; Fan, W.; Ma, Z. C.; Wu, C. T.; Fang, W.; Liu, G.; Xiao, Y. The effects of pore architecture in silk fibroin scaffolds on the growth and differentiation of mesenchymal stem cells expressing BMP7. *Acta Biomater.* **2010**, *6*, 3021−8.

(15) Nair, P. A.; Ramesh, P. Electrospun biodegradable calcium containing poly(ester-urethane)urea: synthesis, fabrication, in vitro degradation, and biocompatibility evaluation. *J. Biomed. Mater. Res., Part A* **2013**, *101*, 1876−1887.

(16) Hong, Y.; Huber, A.; Takanari, K.; Amoroso, N. J.; Hashizume, R.; Badylak, S. F.; Wagner, W. R. Mechanical properties and in vivo behavior of a biodegradable synthetic polymer microfiber-extracellular matrix hydrogel biohybrid scaffold. *Biomaterials* **2011**, *32*, 3387−94.
(17) Hollister, S. J. Porous scaffold design for tissue engineering. *Nat. Mater.* **2005**, *4*, 518−24.
(18) Liu, W.; Thomopoulos, S.; Xia, Y. Electrospun nanofibers for regenerative medicine. *Adv. Healthcare Mater.* **2012**, *1*, 10−25.
(19) Lu, H. H.; Cooper, J. A., Jr.; Manuel, S.; Freeman, J. W.; Attawia, M. A.; Ko, F. K.; Laurencin, C. T. Anterior cruciate ligament regeneration using braided biodegradable scaffolds: in vitro optimization studies. *Biomaterials* **2005**, *26*, 4805−16.
(20) Fang, Y.; Zhang, T.; Zhang, L.; Gong, W.; Sun, W. Biomimetic design and fabrication of scaffolds integrating oriented micro-pores with branched channel networks for myocardial tissue engineering. *Biofabrication* **2019**, *11*, 035004.
(21) McKenna, E.; Klein, T. J.; Doran, M. R.; Futrega, K. Integration of an ultra-strong poly(lactic-co-glycolic acid) (PLGA) knitted mesh into a thermally induced phase separation (TIPS) PLGA porous structure to yield a thin biphasic scaffold suitable for dermal tissue engineering. *Biofabrication* **2020**, *12*, 015015.
(22) Akbarzadeh, R.; Yousefi, A. M. Effects of processing parameters in thermally induced phase separation technique on porous architecture of scaffolds for bone tissue engineering. *J. Biomed. Mater. Res., Part B* **2014**, *102*, 1304−15.
(23) Wu, Y.; Han, Y.; Wong, Y. S.; Fuh, J. Y. H. Fibre-based scaffolding techniques for tendon tissue engineering. *J. Tissue Eng. Regener. Med.* **2018**, *12*, 1798−1821.
(24) Zhang, B.; Guo, L.; Chen, H.; Ventikos, Y.; Narayan, R. J.; Huang, J. Finite element evaluations of the mechanical properties of polycaprolactone/hydroxyapatite scaffolds by direct ink writing: Effects of pore geometry. *J. Mech Behav Biomed Mater.* **2020**, *104*, 103665.
(25) Wu, L.; Magaz, A.; Darbyshire, A.; Howkins, A.; Reynolds, A.; Boyd, I. W.; Song, H.; Song, J. H.; Loizidou, M.; Emberton, M.; Birchall, M.; Song, W. Thermoresponsive Stiffness Softening of Hierarchically Porous Nanohybrid Membranes Promotes Niches for Mesenchymal Stem Cell Differentiation. *Adv. Healthcare Mater.* **2019**, *8*, No. e1801556.
(26) Fang, Y. C.; Zhang, T.; Zhang, L.; Gong, W. F.; Sun, W. Biomimetic design and fabrication of scaffolds integrating oriented micro-pores with branched channel networks for myocardial tissue engineering. *Biofabrication* **2019**, *11*, 035004.
(27) Zheng, Z. F.; Ran, J. S.; Chen, W. S.; Hu, Y. J.; Zhu, T.; Chen, X.; Yin, Z.; Heng, B. C.; Feng, G.; Le, H. H.; Tang, C. Q.; Huang, J. Y.; Chen, Y. W.; Zhou, Y. T.; Dominique, P.; Shen, W. L.; Ouyang, H. W. Alignment of collagen fiber in knitted silk scaffold for functional massive rotator cuff repair. *Acta Biomater.* **2017**, *51*, 317−329.
(28) Zhu, T. H.; Yu, K.; Bhutto, M. A.; Guo, X. R.; Shen, W.; Wang, J.; Chen, W. M.; El-Hamshary, H.; Al-Deyab, S.; Mo, X. M. Synthesis of RGD-peptide modified poly(ester-urethane) urea electrospun nanofibers as a potential application for vascular tissue engineering. *Chem. Eng. J.* **2017**, *315*, 177−190.
(29) Gupte, M. J.; Swanson, W. B.; Hu, J.; Jin, X.; Ma, H.; Zhang, Z.; Liu, Z.; Feng, K.; Feng, G.; Xiao, G.; Hatch, N.; Mishina, Y.; Ma, P. X. Pore size directs bone marrow stromal cell fate and tissue regeneration in nanofibrous macroporous scaffolds by mediating vascularization. *Acta Biomater.* **2018**, *82*, 1−11.
(30) Yang, W.; Xu, H. J.; Lan, Y.; Zhu, Q.; Liu, Y.; Huang, S. S.; Shi, S. G.; Hancharou, A.; Tang, B.; Guo, R. Preparation and characterisation of a novel silk fibroin/hyaluronic acid/sodium alginate scaffold for skin repair. *Int. J. Biol. Macromol.* **2019**, *130*, 58−67.
(31) Oh, J. H.; Park, M. S.; Rhee, S. M. Treatment Strategy for Irreparable Rotator Cuff Tears. *Clin Orthop Surg* **2018**, *10*, 119−134.
(32) Lewington, M. R.; Ferguson, D. P.; Smith, T. D.; Burks, R.; Coady, C.; Wong, I. H. Graft Utilization in the Bridging Reconstruction of Irreparable Rotator Cuff Tears: A Systematic Review. *Am. J. Sports Med.* **2017**, *45*, 3149−3157.
(33) Jones, C. R.; Snyder, S. J. Massive Irreparable Rotator Cuff Tears: A Solution That Bridges the Gap. *Sports Med. Arthrosc Rev.* **2015**, *23*, 130−8.
(34) Nho, S. J.; Delos, D.; Yadav, H.; Pensak, M.; Romeo, A. A.; Warren, R. F.; MacGillivray, J. D. Biomechanical and biologic augmentation for the treatment of massive rotator cuff tears. *Am. J. Sports Med.* **2010**, *38*, 619−29.
(35) Longo, U. G.; Lamberti, A.; Rizzello, G.; Maffulli, N.; Denaro, V. Synthetic augmentation in massive rotator cuff tears. *Med. Sport Sci.* **2011**, *57*, 168−177.
(36) Ker, D. F. E.; Wang, D.; Behn, A. W.; Wang, E. T. H.; Zhang, X.; Zhou, B. Y.; Mercado-Pagan, A. E.; Kim, S.; Kleimeyer, J.; Gharaibeh, B.; Shanjani, Y.; Nelson, D.; Safran, M.; Cheung, E.; Campbell, P.; Yang, Y. P. Functionally Graded, Bone- and Tendon-Like Polyurethane for Rotator Cuff Repair. *Adv. Funct. Mater.* **2018**, *28*, 1707107.
(37) Calejo, I.; Costa-Almeida, R.; Reis, R. L.; Gomes, M. E. Enthesis Tissue Engineering: Biological Requirements Meet at the Interface. *Tissue Eng., Part B* **2019**, *25*, 330−356.
(38) Park, G. Y.; Kwon, D. R.; Lee, S. C. Regeneration of Full-Thickness Rotator Cuff Tendon Tear After Ultrasound-Guided Injection With Umbilical Cord Blood-Derived Mesenchymal Stem Cells in a Rabbit Model. *Stem Cells Transl. Med.* **2015**, *4*, 1344−51.
(39) Min, H. K.; Oh, S. H.; Lee, J. M.; Im, G. I.; Lee, J. H. Porous membrane with reverse gradients of PDGF-BB and BMP-2 for tendon-to-bone repair: in vitro evaluation on adipose-derived stem cell differentiation. *Acta Biomater.* **2014**, *10*, 1272−9.
(40) Carver, T. J.; Kraeutler, M. J.; Smith, J. R.; Bravman, J. T.; McCarty, E. C. Nonarthroplasty Surgical Treatment Options for Massive, Irreparable Rotator Cuff Tears. *Orthop J. Sports Med.* **2018**, *6*, DOI: 10.1177/2325967118805385.
(41) Novi, M.; Kumar, A.; Paladini, P.; Porcellini, G.; Merolla, G. Irreparable rotator cuff tears: challenges and solutions. *Orthop. Res. Rev.* **2018**, *10*, 93−103.
(42) Ghanbar, H.; Luo, C. J.; Bakhshi, P.; Day, R.; Edirisinghe, M. Preparation of porous microsphere-scaffolds by electrohydrodynamic forming and thermally induced phase separation. *Mater. Sci. Eng., C* **2013**, *33*, 2488−98.
(43) Guo, J.; Liu, X. F.; Lee Miller, A., 2nd; Waletzki, B. E.; Yaszemski, M. J.; Lu, L. Novel porous poly(propylene fumarate-co-caprolactone) scaffolds fabricated by thermally induced phase separation. *J. Biomed. Mater. Res., Part A* **2017**, *105*, 226−235.
(44) Liu, W. Y.; Lipner, J.; Xie, J. W.; Manning, C. N.; Thomopoulos, S.; Xia, Y. N. Nanofiber scaffolds with gradients in mineral content for spatial control of osteogenesis. *ACS Appl. Mater. Interfaces* **2014**, *6*, 2842−9.
(45) Zhao, S.; Peng, L. J.; Xie, G. M.; Li, D. F.; Zhao, J. Z.; Ning, C. Q. Effect of the Interposition of Calcium Phosphate Materials on Tendon-Bone Healing During Repair of Chronic Rotator Cuff Tear. *Am. J. Sports Med.* **2014**, *42*, 1920−9.
(46) Zhang, M. Y.; Zhen, J.; Zhang, X.; Yang, Z.; Zhang, L.; Hao, D.; Ren, B. Effect of Autologous Platelet-Rich Plasma and Gelatin Sponge for Tendon-to-Bone Healing After Rabbit Anterior Cruciate Ligament Reconstruction. *Arthroscopy* **2019**, *35*, 1486−1497.
(47) Smith, R. D. J.; Zargar, N.; Brown, C. P.; Nagra, N. S.; Dakin, S. G.; Snelling, S. J. B.; Hakimi, O.; Carr, A. Characterizing the macro and micro mechanical properties of scaffolds for rotator cuff repair. *J. Shoulder Elbow Surg* **2017**, *26*, 2038−2046.
(48) Deymier, A. C.; Schwartz, A. G.; Cai, Z.; Daulton, T. L.; Pasteris, J. D.; Genin, G. M.; Thomopoulos, S. The multiscale structural and mechanical effects of mouse supraspinatus muscle unloading on the mature enthesis. *Acta Biomater.* **2019**, *83*, 302−313.
(49) Foyt, D. A.; Taheem, D. K.; Ferreira, S. A.; Norman, M. D. A.; Petzold, J.; Jell, G.; Grigoriadis, A. E.; Gentleman, E. Hypoxia impacts human MSC response to substrate stiffness during chondrogenic differentiation. *Acta Biomater.* **2019**, *89*, 73−83.
(50) Gugerell, A.; Kober, J.; Laube, T.; Walter, T.; Nurnberger, S.; Gronniger, E.; Bronneke, S.; Wyrwa, R.; Schnabelrauch, M.; Keck, M. Electrospun poly(ester-Urethane)- and poly(ester-Urethane-Urea)

fleeces as promising tissue engineering scaffolds for adipose-derived stem cells. *PLoS One* **2014**, *9*, No. e90676.
(51) Lam, P. H.; Hansen, K.; Keighley, G.; Hackett, L.; Murrell, G. A. A Randomized, Double-Blinded, Placebo-Controlled Clinical Trial Evaluating the Effectiveness of Daily Vibration After Arthroscopic Rotator Cuff Repair. *Am. J. Sports Med.* **2015**, *43*, 2774−82.

https://dx.doi.org/10.1021/acsbiomaterials.0c00193
ACS Biomater. Sci. Eng. 2021, 7, 904−915